Multinucleon transfer in the ^{116}Cd(^{20}Ne, ^{20}O)^{116}Sn double charge exchange reaction at 306 MeV incident energy

J. L. Ferreira,[1] J. Lubian,[1] F. Cappuzzello,[2,3] M. Cavallaro,[2] and D. Carbone[2]
(NUMEN Collaboration)
[1]*Instituto de Física, Universidade Federal Fluminense, Niterói, Rio de Janeiro 24210-340, Brazil*
[2]*Istituto Nazionale di Fisica Nucleare - Laboratori Nazionali del Sud, via S. Sofia 62, 95123, Catania, Italy*
[3]*Dipartimento di Fisica e Astronomia "Ettore Majorana", University of Catania, via Santa Sofia 64, 95123, Catania, Italy*

(Received 8 November 2021; accepted 14 January 2022; published 31 January 2022)

In heavy-ion collisions at energies above the Coulomb barrier, the multiple nucleon transfer mechanism feeding double charge exchange (DCE) reactions can compete with the meson-induced DCE process once, in both cases, the same final partition is achieved. While the former is a mean field driven process, the latter is generated by second-order isovector components of the nucleon-nucleon interaction. It is particularly interesting to isolate the meson-induced DCE from measured cross sections since their matrix elements can be linked to those controlling the expected double β decay rates. However, one needs first to isolate the meson-induced DCE contribution, which in turn means that careful scrutiny of the DCE flux from the multinucleon transfer is mandatory. This work presents theoretical results for all the multinucleon transfer routes feeding the ^{116}Cd(^{20}Ne, ^{20}O)^{116}Sn reaction at 306 MeV incident energy. The calculated cross sections are obtained considering the distorted wave Born approximation and coupled channel Born approximation, where the role of the couplings with inelastic states in the initial partition is discussed. Moreover, the spectroscopic amplitudes for the projectile and target overlaps are extracted by considering a large-scale shell-model calculation.

DOI: 10.1103/PhysRevC.105.014630

I. INTRODUCTION

Nowadays, a great effort is being carried out in analyzing double charge exchange (DCE) reactions both from the experimental and theoretical points of view [1–10]. The reason is that the matrix element of this class of reactions may be associated with those entering in the double-β decay process. The main objective of many of these studies has been to provide precise information about the nuclear matrix element of the meson-induced correlated DCE transition [8], which has typical features of the one corresponding to the hypothetical neutrinoless double-β decay ($0\nu\beta\beta$) phenomenon [1,3,8,9].

From the theoretical side, recent studies [8] have shown that a particular class of diagrams, where two correlated isovector mesons are exchanged by target and projectile in a DCE reaction, is particularly interesting. This reaction mechanism, called the Majorana mechanism, requires a single-step action of the initial (ISI) and final (FSI) state nucleus-nucleus interaction. The form factor is based on the isotensor component of the short-range nucleon-nucleon correlations, thus probing a similar nuclear response as the high-momentum neutrinoless double beta decay operators.

However, DCE reactions can also be promoted by low-momentum nucleon-nucleon isovector interaction through the exchange of two uncorrelated mesons. In this case, two direct meson exchange single charge exchange processes (SCE) will occur sequentially, thus requiring a two-step action of the ISI and FSI. Also, the study of this DCE mechanism is promising, but more in connection to two-neutrino double-β decay matrix elements [9,11]. Finally, the DCE reactions are also allowed with the actual transfer of nucleons (two protons and two neutrons) between the target and projectile. These mechanisms are of multistep character in the ISI and FSI. In this case, the form factors are built on the nucleon-nucleus mean field. Despite multinucleon transfer DCE mechanisms are not directly connected to neutrinoless double-β decay studies, it is very important to carefully study them for two main reasons. First, as they contribute to the measured DCE cross sections, it is vital to know their weight and look for experimental conditions where they can be minimized. Second, they provide additional information on the nuclear states involved in double-β decays. Namely, single-particle orbitals and nucleon-nucleon pairing correlations can be explored for bound and resonant states, also with the help of data accessible in the experiments.

In this framework, the nuclear matrix element for neutrinoless double-β decay (NUMEN) project [1,2] has recently proposed to explore (^{18}O, ^{18}Ne), (^{20}Ne, ^{20}O), and (^{12}C, ^{12}Be) DCE reactions for all targets of interest for double-β decay research. Also, the nuclear reaction for neutrinoless double beta decay (NURE) project is moving along this line [7]. Both NUMEN and NURE are focusing on incident energies in the range 10–60 MeV/u. Slightly different approaches are being proposed in Japan, where the main focus is on the search of double Gamow-Teller giant resonance by DCE and the experiments are performed at higher incident energies ($>$100 MeV/u) [6].

As stated before, whatever is the dominant DCE mechanism, the ISI and FSI are key elements and should be known

in detail. The use of double folding potentials, where the densities of the projectile and target nuclei are folded with the nucleon-nucleon interaction, was proven to be adequate for this purpose. The most accurate results are achieved when elastic scattering data are collected to directly compare ISI and FSI with experimental data [12–19]. The possible measurement of inelastic scattering cross sections allows to consistently extend the ISI and FSI to account for the excitations of the colliding nuclei before or after the reaction [8,16].

When moving to nucleon transfer reactions, one should also deal with nuclear structure inputs, expressed by the spectroscopic amplitudes, representing the overlaps of the nuclear states with specific configurations, preferentially excited by the reaction. For example, single-particle spectroscopic amplitudes are necessary to study one-nucleon transfer reactions.

One- and two-nucleon (or even multinucleon) transfer reactions have extensively been studied in the last few years [20–31]. These peripheral reactions, which are highly selective between the initial and final states populated by the transferred nucleon (or nucleons), have shown to be essential tools to probe the structure of nuclei. In particular, two-neutron transfer [13,14,32–44] and, more recently, two-proton transfer [44–46] reactions were studied. The theoretical prescription used to determine angular distributions and integrated cross sections provided a very good agreement with the experimental data. This prescription, already well tested in these works, will be used in the present work to determine the multi-nucleon transfer cross sections.

These studies aimed to gather information about the single- and two-particle characteristics of the states populated by the transferred particles and the relationship between the transfer mechanisms (direct or sequential) involved in the two-particle transfer reactions. Also, the collectivity of the states populated by the two transferred particles was put in evidence. The low-energy excited states with high collectivity were preferably populated by sequential two-particle transfer [15,30,31,39,45]. Besides, in the cases where also the elastic scattering cross sections were measured, the used optical potentials provided a very good description of both elastic scattering and transfer angular distributions [12–19,28,29]. Thus our methodology including the use of double folding optical potentials is able predict the transfer cross sections with reasonable accuracy even when elastic scattering data are not available. This is a critical condition for some of the systems that will be analyzed in the NUMEN project.

Despite the fact that several studies have been performed for nucleon transfer reactions, the contribution to specific DCE transitions has not been explored so far in a quantitative approach. In Ref. [2] it is stated that multinucleon transfer driven by an initial step with a two-proton or two-neutron transfer gives a negligible contribution to DCE for the case of ^{18}O(^{40}Ca, ^{40}Ar) ^{18}Ne reaction at 15 MeV/u. However, the conclusion of Ref. [2] is based on a rather qualitative argument, and no calculations were performed. Other studies of multinucleon transfer in heavy-ion collisions have been reported with analyses based on semiclassical approaches and focused on energy-integrated cross sections [47–50]. In such other cases, no information about individual DCE transitions is discussed.

Here, we present, a comprehensive theoretical study of the multinucleon transfer mechanisms in the ^{116}Cd(^{20}Ne, ^{20}O)^{116}Sn DCE reaction, at 306 MeV incident energy, competing with the direct DCE process. We also discuss the role played by the coupling with excited states of the projectile and target nuclei in this reaction. In Ref. [44], the importance of such couplings for the two-proton stripping and two-neutron pickup reactions in the ^{20}Ne + ^{116}Cd collision at 306 MeV incident energy was reported.

The techniques adopted in Ref. [44] for the two-proton and two-neutron transfer channels are extended here up to the fourth order to describe the full net of transfer channels feeding the DCE cross section. In particular, large-scale shell-model calculations are performed to obtain the one- and two-nucleon spectroscopic amplitudes related to the projectile and target overlaps considered in the present multinucleon transfer reactions.

The transfer channels are treated perturbatively in the Born approximation. The double folding São Paulo potential [51,52] is used in the real and imaginary parts of the optical potential both for the ISI and FSI. No arbitrary scaling factor is considered to make the theoretical results closest to the experimental data when available, as usually done in the past [53–56].

The calculations presented here are fully compatible with those of Ref. [44] for the two-nucleon transfer channel and of Ref. [19] for the elastic, inelastic, one-proton transfer, and single charge exchange channels, since the same ingredients have been used. Thus, the comparison with the data there shown gives a confirmation of the reliability of our calculations to the unknown double charge exchange cross sections.

This paper is organized as follows. The theoretical discussions are presented in Sec. II and the conclusions are given in Sec. III.

II. RESULTS AND DISCUSSION

Multinucleon transfer reaction cross sections in the ^{20}Ne + ^{116}Cd collision at 306 MeV incident energy were determined within the distorted wave (DWBA) and coupled channels (CCBA) Born approximation approaches, using the FRESCO code [57,58]. We mainly aim to analyze the relevance of each transfer route in the ^{116}Cd(^{20}Ne, ^{20}O)^{116}Sn reaction, which might compete with the direct double charge exchange (DCE) reaction.

Some ingredients are necessary to perform these calculations, such as optical potentials for the ISI and FSI, spectroscopic amplitudes, reduced electric transition probabilities, and deformation lengths to access the collective modes.

In all partitions considered in the present multinucleon transfer calculation, the São Paulo potential [51,52] was considered as the real and imaginary parts of the optical potential. The following normalization coefficients $U(\mathbf{R}) = (1.0 + 0.78i)V_{\rm LE}^{\rm SPP}(\mathbf{R})$ [59,60] were used when the couplings with inelastic states into the partition were disregarded. Following the prescription of Refs. [13,32,36–39,41,61–63], the normalization factor 0.6 is used in the imaginary part when the couplings with relevant inelastic channels are explicitly included in the system of coupled equations.

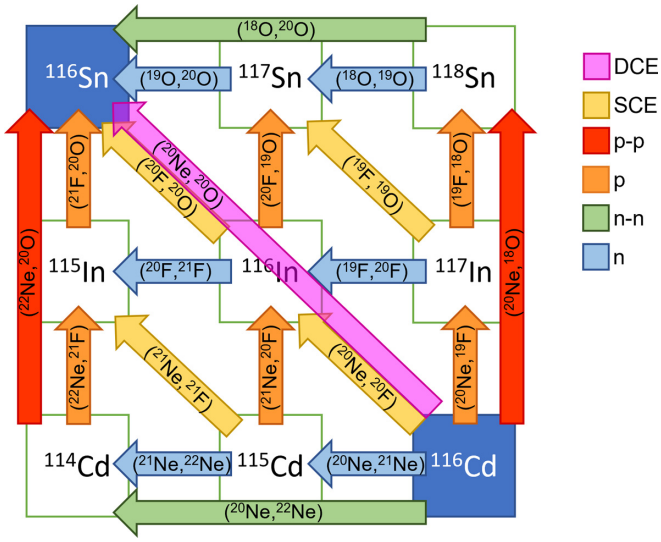

FIG. 1. Scheme of possible transfer reactions that would reach in the same final partition reached by the direct DCE process. Each reaction mechanism is identified with one color.

The São Paulo potential is a local-equivalent double folding potential expressed as

$$V_{\rm LE}^{\rm SPP}(\mathbf{R}) = \int \rho(\mathbf{r}_1) V(\mathbf{R} - \mathbf{r}_1 + \mathbf{r}_2) \rho(\mathbf{r}_2) e^{-4v^2/c^2} d\mathbf{r}_1 d\mathbf{r}_2, \tag{1}$$

that takes into account a nucleon-nucleon M3Y interaction [64,65] represented by $V(\mathbf{R} - \mathbf{r}_1 + \mathbf{r}_2)$. In this expression, the appearance of the e^{-4v^2/c^2} term is related to the transformation of nonlocal into a local-equivalent potential, where $v^2 = \frac{2}{\mu}[E - V_C(\mathbf{R}) - V_{\rm LE}^{\rm SPP}(\mathbf{R})]$ is the relative velocity of the interaction ions and c is the vacuum speed of light. Also, $V_C(\mathbf{R})$ is the Coulomb potential and μ the reduced mass of the system. Thus, the local-equivalent potential $V_{\rm LE}^{\rm SPP}(\mathbf{R})$ is connected to a folding potential $V_F(\mathbf{R}) = \int \rho(\mathbf{r}_1) V(\mathbf{R} - \mathbf{r}_1 + \mathbf{r}_2) \rho(\mathbf{r}_2) d\mathbf{r}_1 d\mathbf{r}_2$. In this context, it is also possible to consider the exponential term in Eq. (1) as the absolute normalization of the folding potential $V_{\rm LE}^{\rm SPP}(\mathbf{R}) = V_F(\mathbf{R}) e^{-4v^2/c^2}$ [51,52,61]. In Ref. [66], the authors consider the nucleon-nucleon M3Y interaction to study the proprieties of asymmetric nuclear matter. This study considered realistic density dependence of the original nucleon-nucleon M3Y interaction. However, in the present work, this approach was not adopted.

The matter densities of the collision partner nuclei are determined by using the two parameters Fermi Dirac distribution

$$\rho(r) = \frac{\rho_0}{1 + \exp\left(\frac{r - R_0}{a}\right)} \tag{2}$$

with radius $R_0 = (1.31A^{1/3} - 0.81)$ fm and matter diffuseness $a = 0.56$ fm. In addition, ρ_0 can be determined from the normalization condition for the matter density $4\pi \int \rho(r) r^2 dr = A$, where A is the mass number of the nucleus.

In Fig. 1, the different paths that lead to the same final partition as the direct DCE reaction are shown. There are many multinucleon transfer paths for the ^{20}Ne + ^{116}Cd → ^{20}O + ^{116}Sn transition to be considered in the calculations. In principle, all those processes shown in Fig. 1 may coexist during the reaction competing with each other. The transfer amplitudes for each of them should be coherently summed to obtain the angular distributions for the transitions to the different states populated in the final partition. In the present work, we are interested in performing multinucleon transfer calculations for those paths, separately, that only involve the transfer of nucleons. Therefore, the paths for which the transfer of nucleons is preceded or followed by a single charge exchange process will not be considered, although these processes might also compete with the direct DCE reaction [1,2,8,9].

The direct two-neutron or two-proton transfer reactions are analyzed by considering the independent coordinate scheme, where Woods-Saxon potentials generate the single-particle wave function of each valence nucleon. A transformation of coordinates is then performed to convert the independent coordinates of both valence nucleons into the center of mass coordinate of the two nucleons and the relative motion coordinate. This methodology for the direct two-particle transfer has extensively been used in Refs. [13,14,36–39,44,45].

Another possibility is that the two neutrons (or protons) are transferred one by one passing through an intermediate partition. In this case, to achieve the final partition ^{20}O + ^{116}Sn, the transfer process would be performed by four steps and would correspond to the nucleons exchange between projectile and target nuclei, keeping their mass number unchanged. Of course, a three-step DCE process is possible: two nucleons are transferred together; the other two nucleons are transferred sequentially. The geometric parameters of the Woods-Saxon potentials, used to generate the single-particle wave functions, corresponding to the bound states of each valence nucleon, were $r = 1.26$ fm and $a = 0.70$ fm for the lighter nuclei, and $r = 1.20$ fm and $a = 0.60$ fm for the heavier nuclei, thus following a well-established parametrization [13,36–38,41,44,45].

In Fig. 2, the coupling schemes for the ^{116}Cd(^{20}Ne, ^{20}O)^{116}Sn reaction occurring by direct two-proton stripping transfer followed by direct two-neutron pickup process is shown. In Fig. 3, the direct two-neutron pickup followed by the two-proton stripping is represented. The figures of coupling schemes for the other routes were omitted here to avoid overloading the paper. We prefer to show the coupling scheme of these two reactions paths since they have larger cross sections. Instead of coupling schemes, we show a table (see Table I) for the excited states included in all the partitions. All the possible couplings were considered.

The transfer matrix elements were determined using the prior representation of the potential and considering the nonorthogonality correction. The one- and two-particle spectroscopic amplitudes for the projectile and target overlaps were derived from shell-model calculations using the NUSHELLX code [67].

The spectroscopic amplitudes for the projectile overlaps were determined considering the phenomenological *p-sd-mod* [68] interaction, which considers an alpha particle as a closed core. Moreover, the orbits $1p_{3/2}$, $1p_{1/2}$, $1d_{5/2}$, $2s_{1/2}$, and $1d_{3/2}$

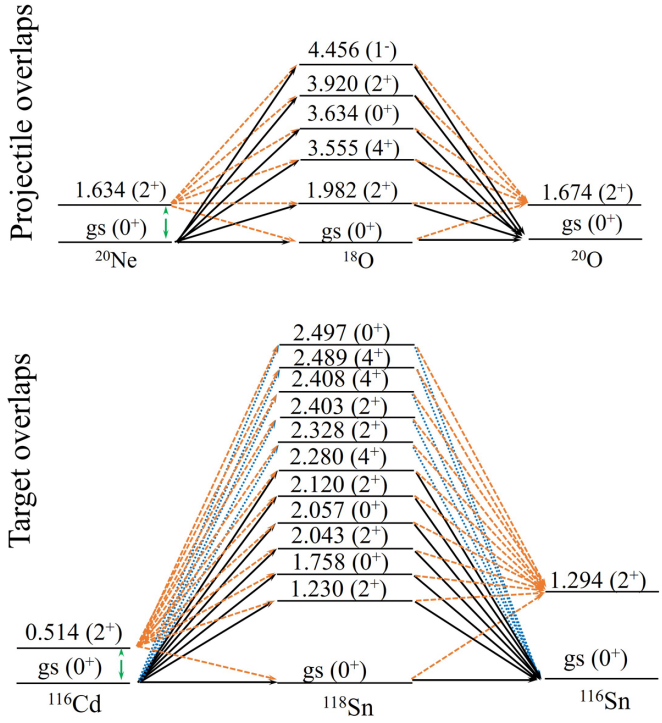

FIG. 2. Coupling scheme considered in the direct two-proton stripping transfer followed by the direct two-neutron pickup transfer reactions.

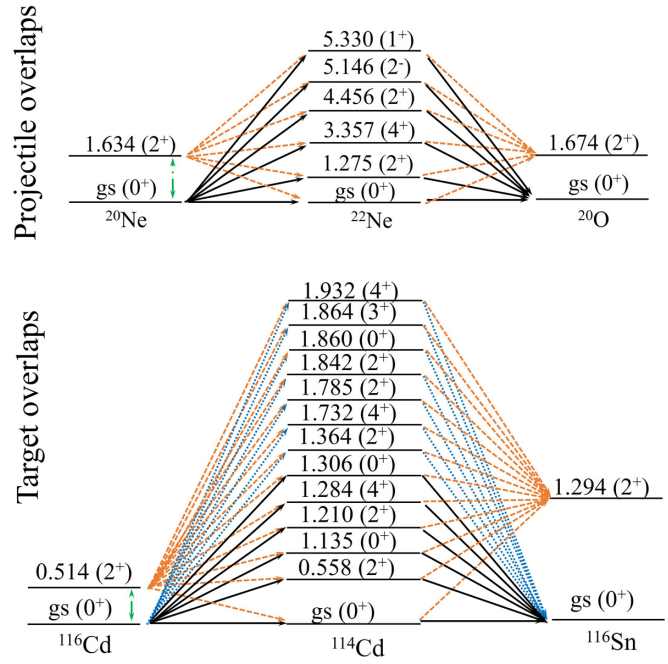

FIG. 3. Coupling scheme considered in the direct two-neutron pickup transfer followed by the direct two-proton stripping transfer reactions.

were considered as model space for both proton and neutron valence particles. This interaction has successfully described the structural characteristic of the lowest states of the ^{16,17,18}O isotopes. We have used this interaction to obtain spectroscopic amplitudes for the ^{13,14,15}C isotopes to study the two-neutron transfer reaction in the $^{18}\mathrm{O} + {}^{13}\mathrm{C}$ collision at 84 MeV incident energy [38]. More recently, we have also achieved a good description of the experimental cross sections for the two-proton and two-neutron transfer in the $^{20}\mathrm{Ne} + {}^{116}\mathrm{Cd}$ collision [44] at 306 MeV incident energy.

The structure information for the medium-heavy target (and residual) nuclei was obtained considering the effective residual interaction *jj45pna* [69] in the shell-model Hamiltonian. The structure model space in which this interaction was elaborated considers the valence orbits $1f_{5/2}$, $2p_{3/2}$, $2p_{1/2}$, and $1g_{9/2}$ for protons and $1g_{7/2}$, $2d_{5/2}$, $2d_{3/2}$, $3s_{1/2}$, and $1h_{11/2}$ for neutrons. The proton-proton, neutron-neutron, and proton-neutron components of this interaction were derived from the charge-dependent Bonn potential (CD-Bonn) [70,71]. Recently, we have used this effective interaction to obtain the one-, and two-nucleon spectroscopic amplitudes for the target overlaps involved in the ^{116}Cd(^{20}Ne, ^{18}O) ^{118}Sn and ^{116}Cd(^{20}Ne, ^{22}Ne) ^{114}Cd reactions [44], at 306 MeV incident energy.

Although the one- and two-nucleon spectroscopic amplitudes were not explicitly presented in this work, most of them can be accessed in Refs. [44,45]. The others are obtained from shell model calculations by using the effective interactions mentioned above, which are standard interactions in NUSHELLX code [67].

In Fig. 4, we show the results for the angular distributions for the transitions to the $^{20}\mathrm{O}_{\mathrm{g.s.}} + {}^{116}\mathrm{Sn}_{\mathrm{g.s.}}$ channel, corresponding to each route illustrated in Fig. 1, and concerning the couplings represented by the full black arrows in Figs. 2 and 3. That is, considering some low-lying states in the intermediate partitions of each possible path for which the transfer reaction occurs. Figure 4(a) shows the angular distributions of processes starting with one- or two-proton transfer. Conversely, Fig. 4(b) contains the angular distributions in which the first step is the one- or two-neutron transfer process. Notice that the sequential two-proton (two-neutron) transfer is represented by *p*-*p* (*n*-*n*), while the direct two-proton (two-neutron) transfer is by 2*p* (2*n*).

The theoretical results shown in Fig. 4 indicate that, in most cases, the processes initiated by one- or two-neutron transfer have cross sections larger than those in which one or two protons are initially transferred (especially at forward angles). In Ref. [44], the experimental data show that the stripping of two protons populating the lowest states in the $^{20}\mathrm{Ne} + {}^{116}\mathrm{Cd} \rightarrow {}^{18}\mathrm{O} + {}^{118}\mathrm{Sn}$ reaction is suppressed when compared to the $^{20}\mathrm{Ne} + {}^{116}\mathrm{Cd} \rightarrow {}^{22}\mathrm{Ne} + {}^{114}\mathrm{Cd}$ two-neutron pickup reaction. This might be associated with the kinematic conditions for charged particle transfer that can preferably populate higher excited states in the ^{118}Sn nucleus [72]. In Ref. [44], the experimental energy spectrum of the two-proton stripping reaction ^{116}Cd(^{20}Ne, ^{18}O) ^{118}Sn is shown. The energy spectrum has a bump for the ^{118}Sn states at an excitation energy $E_x = Q_0 - Q = 15$ MeV, where Q_0 and Q stand for the reaction Q value for the transition to the ground and to the excited state, respectively. This could make an unfavorable environment accessing the $^{20}\mathrm{O} + {}^{116}\mathrm{Sn}$ channel in the second step of the multinucleon transfer in the $^{18}\mathrm{O} + {}^{118}\mathrm{Sn}$

TABLE I. Eigenstates [E(MeV); (I^{π})] of the light and heavy nuclei considered in the coupling schemes of the multi-nucleon transfer DCE calculations.

^{20}Ne	^{21}Ne	^{22}Ne	^{20}O	^{19}O	^{18}O	^{19}F	^{20}F	^{21}F
0.0(0^+)	0.0 ($3/2^+$)	0.0 (0^+)	0.0 (0^+)	0.0 ($5/2^+$)	0.0 (0^+)	0.0 ($1/2^+$)	0.0 (2^+)	0.0 ($5/2^+$)
1.624(2^+)	0.351 ($5/2^+$)	1.275 (2^+)	1.674 (2^+)	0.096 ($3/2^+$)	1.980 (2^+)	0.110 ($1/2^-$)	0.656 (3^+)	0.280 ($1/2^+$)
	1.746 ($7/2^+$)	3.357 (4^+)		1.472 ($1/2^+$)	3.555 (4^+)	0.197 ($5/2^+$)	0.823 (4^+)	1.101 ($1/2^-$)
	2.789 ($1/2^-$)	4.456 (2^+)		2.372 ($9/2^+$)	3.634 (0^+)	1.346 ($5/2^-$)	0.984 (1^-)	1.730 ($3/2^+$)
	2.794 ($1/2^+$)	5.146 (2^-)		2.779 ($7/2^+$)	3.920 (2^+)	1.459 ($3/2^-$)	1.057 (1^+)	2.040 ($3/2^-$)
	2.867 ($9/2^+$)					1.554 ($3/2^+$)		
^{116}Cd	^{115}Cd	^{114}Cd	^{116}Sn	^{117}Sn	^{118}Sn	^{115}In	^{116}In	^{117}In
0.0 (0^+)	0.0 ($1/2^+$)	0.0 (0^+)	0.0 (0^+)	0.0 ($1/2^+$)	0.0 (0^+)	0.0 ($9/2^+$)	0.0 (1^+)	0.0 ($9/2^+$)
0.514(2^+)	0.229 ($3/2^+$)	0.558 (2^+)	1.294 (2^+)	0.159 ($3/2^+$)	1.230 (2^+)	0.336 ($1/2^-$)	0.128 (5^+)	0.315 ($1/2^-$)
	0.361 ($5/2^+$)	1.135 (0^+)		0.712 ($7/2^+$)	1.758 (0^+)	0.597 ($3/2^-$)	0.223 (4^+)	0.589 ($3/2^-$)
	0.390 ($7/2^+$)	1.210 (2^+)		1.005 ($3/2^+$)	2.043 (2^+)	0.829 ($3/2^+$)	0.273 (2^+)	0.748 ($7/2^+$)
	0.473 ($3/2^+$)	1.284 (4^+)		1.020 ($5/2^+$)	2.057 (0^+)	0.864 ($1/2^+$)	0.290 (8^-)	0.881 ($5/2^+$)
	0.507 ($5/2^+$)	1.305 (0^+)		1.180 ($5/2^+$)	2.280 (4^+)	0.934 ($7/2^+$)	0.313 (4^+)	1.028 ($5/2^-$)
	0.649 ($1/2^+$)	1.364 (2^+)		1.446 ($5/2^+$)	2.328 (2^+)	0.941 ($5/2^+$)		1.052 ($5/2^+$)
	0.749 ($3/2^+$)	1.732 (4^+)		1.469 ($3/2^+$)	2.403 (2^+)	1.041 ($5/2^-$)		1.360 ($5/2^+$)
	0.777 ($5/2^+$)	1.785 (2^+)		1.469 ($5/2^+$)	2.408 (4^+)	1.133 ($11/2^+$)		1.366 ($9/2^+$)
	0.804 ($1/2^+$)	1.842 (4^+)		1.497 ($5/2^+$)	2.489 (4^+)	1.287 ($3/2^-$)		1.433 ($9/2^+$)
	0.963 ($1/2^+$)	1.860 (0^+)		1.530 ($3/2^+$)	2.497 (0^+)	1.287 ($5/2^-$)		1.469 ($5/2^+$)
	1.062 ($7/2^+$)	1.864 (3^+)		1.578 ($3/2^+$)		1.291 ($13/2^+$)		1.554 ($1/2^-$)
	1.085 ($5/2^+$)	1.932 (4^+)		1.589 ($3/2^+$)		1.347 ($5/2^-$)		1.653 ($5/2^+$)
	1.597 ($5/2^+$)			1.629 ($9/2^+$)		1.418 ($11/2^+$)		1.856 ($5/2^-$)
	1.620 ($5/2^+$)			1.668 ($3/2^+$)		1.448 ($9/2^+$)		1.957 ($9/2^-$)
				1.710 ($5/2^+$)		1.470 ($3/2^-$)		2.113 ($5/2^+$)
				1.770 ($5/2^+$)		1.486 ($9/2^+$)		2.223 ($5/2^+$)
				1.875 ($11/2^+$)		1.602 ($7/2^+$)		2.255 ($5/2^+$)
				2.050 ($9/2^+$)		1.608 ($7/2^+$)		2.308 ($9/2^+$)
				2.079 ($1/2^+$)		1.650 ($3/2^-$)		
				2.146 ($5/2^+$)		1.737 ($9/2^+$)		
				2.300 ($5/2^+$)		1.830 ($5/2^+$)		
				2.400 ($1/2^+$)		1.972 ($9/2^+$)		

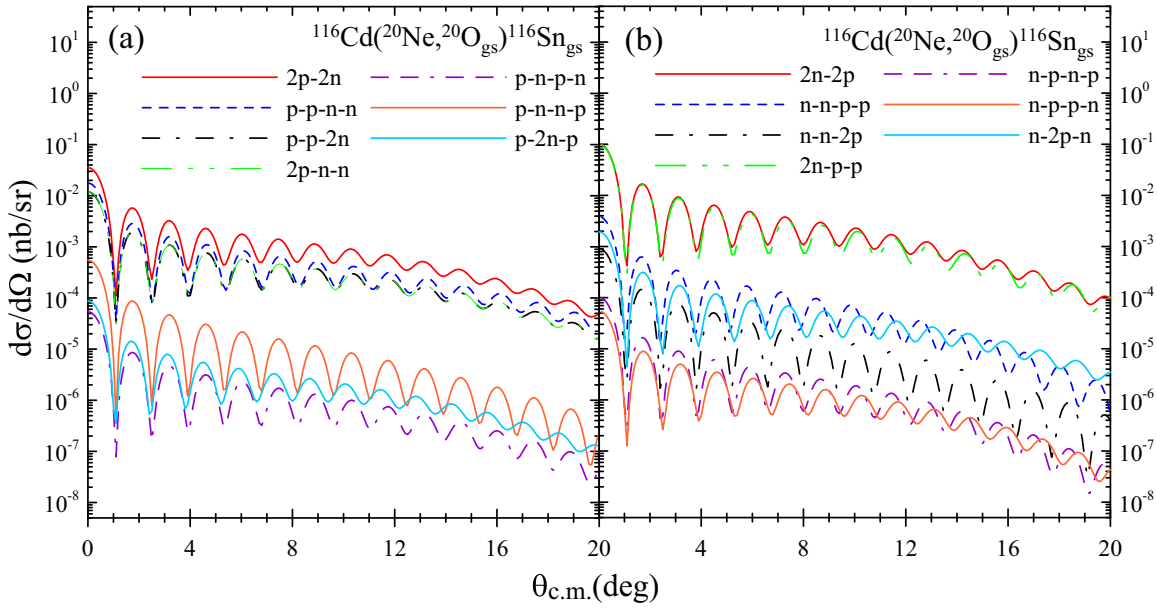

FIG. 4. Theoretical angular distribution for the ^{20}O$_{g.s.}$ + ^{116}Sn$_{g.s.}$ channel corresponding to each route illustrated in Fig. 1. In (a) are the angular distributions for which transfer reaction of nucleons beginning with one- or two-proton transfer. In (b) are the angular distributions for which the transfer reaction of nucleons beginning with one- or two-neutron transfer. The results for the angular distributions are considering few low-lying states of the heavier nuclei represented in Table I.

TABLE II. Integrated cross-sections in the angular range $3^\circ \leqslant \theta_{\rm c.m.} \leqslant 13^\circ$ for each channel that might contribute to the DCE cross-section (see text). The integrated cross-sections are given in nb. The results for the cross sections are considering few low-lying states of the heavier nuclei represented in Table I.

	Final partition		
Mechanism	$^{20}O_{g.s.}(0^+) + {}^{116}Sn_{g.s.}(0^+)$	$^{20}O_{1.67}(2^+) + {}^{116}Sn_{g.s.}(0^+)$	$^{20}O_{g.s.}(0^+) + {}^{116}Sn_{1.23}(2^+)$
$2p-2n$	$1,28 \times 10^{-4}$	$1,82 \times 10^{-4}$	$4,85 \times 10^{-5}$
$2n-2p$	$3,13 \times 10^{-4}$	$1,32 \times 10^{-4}$	$6,76 \times 10^{-5}$
$p-p-n-n$	$6,63 \times 10^{-5}$	$1,01 \times 10^{-4}$	$1,25 \times 10^{-5}$
$n-n-p-p$	$1,00 \times 10^{-5}$	$3,57 \times 10^{-5}$	$2,34 \times 10^{-5}$
$p-p-2n$	$4,15 \times 10^{-5}$	$4,64 \times 10^{-5}$	$2,09 \times 10^{-5}$
$n-n-2p$	$1,72 \times 10^{-6}$	$7,12 \times 10^{-5}$	$2,82 \times 10^{-6}$
$2p-n-n$	$9,26 \times 10^{-5}$	$1,81 \times 10^{-4}$	$3,18 \times 10^{-5}$
$2n-p-p$	$2,66 \times 10^{-4}$	$1,10 \times 10^{-4}$	$1,17 \times 10^{-4}$
$p-n-p-n$	$1,38 \times 10^{-7}$	$1,93 \times 10^{-7}$	$1,44 \times 10^{-7}$
$p-n-n-p$	$1,15 \times 10^{-6}$	$5,35 \times 10^{-7}$	$4,35 \times 10^{-7}$
$n-p-n-p$	$2,53 \times 10^{-7}$	$7,06 \times 10^{-8}$	$1,06 \times 10^{-7}$
$n-p-p-n$	$1,69 \times 10^{-7}$	$4,94 \times 10^{-7}$	$4,18 \times 10^{-7}$
$p-2n-p$	$2,51 \times 10^{-7}$	$9,90 \times 10^{-7}$	$3,58 \times 10^{-7}$
$n-2p-n$	$5,71 \times 10^{-6}$	$2,05 \times 10^{-4}$	$1,72 \times 10^{-5}$
Incoh. Sum	$9,60 \times 10^{-4}$	$1,07 \times 10^{-3}$	$3,43 \times 10^{-4}$

$\rightarrow {}^{20}O + {}^{116}Sn$ transition (see Fig. 1). In addition, since the E_x that maximizes the (^{20}Ne, ^{18}O) cross section is beyond the nucleon emission threshold most of its flux is lost in nucleon emission processes, which cannot feed DCE. Indeed, DCE are charge and mass conserving binary reactions. We comment here that the agreement between experimental cross sections and theoretical results for the two-proton stripping and two-neutron pickup reactions in the $^{20}Ne + {}^{116}Cd$ collision was quite good [44], supporting the feasibility of the theoretical approach to calculate two-particle transfer cross sections.

Table II shows the cross sections integrated in the angular range $3^\circ \leqslant \theta_{\rm c.m.} \leqslant 13^\circ$ in the center of mass framework, for the final DCE channels $^{20}O_{g.s.}(0^+) + {}^{116}Sn_{g.s.}(0^+)$, $^{20}O_{1.67}(2^+) + {}^{116}Sn_{g.s.}(0^+)$, and $^{20}O_{g.s.}(0^+) + {}^{116}Sn_{1.23}(2^+)$ corresponding to each multinucleon transfer path sketched in Fig. 1. As one can observe, these cross sections are very small. The largest cross sections for the transition to the ground states of the final partition, for instance, are about $\approx 10^{-4}$ nb. The experimental integrated cross sections for the $^{116}Cd(^{20}Ne, {}^{20}O)^{116}Sn$ leading to the same transitions are typically some nanobarns. Similar values were measured also for other systems [2,10]. Also, even ignoring the quantum interference effect, Table II shows the incoherent sums of all possible transfer paths seeking the same final partition $^{20}O + {}^{116}Sn$ in the DCE process. As one can observe, the cross section of the transfer DCE gives a negligible contribution to the measured value.

Another important point to mention is the role of couplings to the projectile and target inelastic states on the cross sections of the channels in the final partition. These collective modes are accessed by deforming the Coulomb and nuclear potentials, as a usual approach [73]. The 2_1^+ collective state of the ^{20}Ne is accessed by considering the deformation parameter $\beta = 0.72$ [74] in the rotational model frame. Moreover, for the ^{116}Cd nucleus, the one-phonon (2_1^+) excited state is included explicitly in the coupled equation, in which the used quadrupole deformation parameter is $\beta = 0.19$ [74]. Once we include couplings explicitly with inelastic states in the initial partition, the strength coefficient of the imaginary part of the optical potential N_I was reduced to 0.6 [61–63] to avoid double counting. Besides, to include couplings with the 2_1^+ excited state of both projectile and target in the entrance partition, we also increase the basis of states of the heavier nuclei in the intermediate partitions. Eigenstates with energies up to around 2 MeV for the target-like nuclei were considered in all the intermediate partitions. This choice covers a high density of states for these medium-heavy nuclei in the calculations, although their neutron/proton separation energies are typically higher than 2 MeV.

The couplings schemes considered in the transfer calculations account for additional couplings outlined by the dotted blue, dashed orange, and dashed-dotted green arrows, as shown in Figs. 2 and 3. Table III shows the theoretical cross sections calculated accounting for the full couplings for the transfer processes feeding the same partition reached by the DCE process. Only the cross-sections for the main processes (having larger cross sections) are shown. So, we give the new values for the cross section corresponding to the paths in which both protons and neutrons are simultaneously transferred. We also show the cases where the sequential two-proton (two-neutron) transfer reaction occurs, followed by the sequential two-neutron (two-proton) transfer. As one can see in this table, even including couplings with higher excited states in the intermediate partitions, the order of magnitude remains unchanged.

To give an illustrative example of the effects caused by the inclusion of the couplings represented by the dotted blue, dashed orange, and dashed-dotted green arrows in Figs. 2 and 3, we show in Fig. 5 the theoretical angular distributions

TABLE III. Integrated cross-sections in the angular range $3^\circ \leqslant \theta_{\text{c.m.}} \leqslant 13^\circ$ for each channel that might contribute to the DCE cross-section. These cross-sections are obtained by considering the full coupling schemes sketched in Figs. 2 and 3 (see text). The integrated cross-sections are given in nb.

	Final partition		
Mechanism	$^{20}O_{g.s.}(0^+) + {}^{116}Sn_{g.s.}(0^+)$	$^{20}O_{1.67}(2^+) + {}^{116}Sn_{g.s.}(0^+)$	$^{20}O_{g.s.}(0^+) + {}^{116}Sn_{1.23}(2^+)$
$2p-2n$	$7,83 \times 10^{-4}$	$4,95 \times 10^{-4}$	$2,82 \times 10^{-4}$
$2n-2p$	$2,89 \times 10^{-4}$	$1,27 \times 10^{-4}$	$7,10 \times 10^{-5}$
$p-p-n-n$	$1,86 \times 10^{-4}$	$2,32 \times 10^{-4}$	$3,11 \times 10^{-5}$
$n-n-p-p$	$2,37 \times 10^{-4}$	$4,79 \times 10^{-5}$	$3,32 \times 10^{-5}$

populating the $^{20}O_{g.s.} + {}^{116}Sn_{g.s.}$ channel in the multinucleon transfer reactions. In this figure, the results for the angular distributions characterized by the dotted red curve account for the couplings depicted by the full black arrows in Figs. 2 and 3. The dashed-dotted black curve accounts for the extra couplings to higher excited states in ^{118}Sn and ^{114}Cd, represented by dotted blue arrows in Figs. 2 and 3. The effect generated by including the 2_1^+ excited states of the projectile and target is illustrated in the blue curve of Fig. 5. One notices that the inelastic states in the initial partitions play a relevant role in the DCE multinucleon transfer mechanism. In fact, for these two paths of DCE transfer reactions, the coupling with those 2^+ inelastic states in the initial partition seems to be more relevant than increasing the basis of states of the ^{118}Sn and ^{114}Cd nuclei in the respective intermediate partitions. The two-phonon excited states of the target ^{116}Cd (0_2^+, 2_2^+, 4_1^+) were not included in the present analysis. Since they are accessed through a second-order process, in fact the effects on the angular distribution of the $^{20}O_{g.s.} + {}^{116}Sn_{g.s.}$ channel due to couplings to this two-phonon excited state and the states belonging to the intermediate partition should be weak.

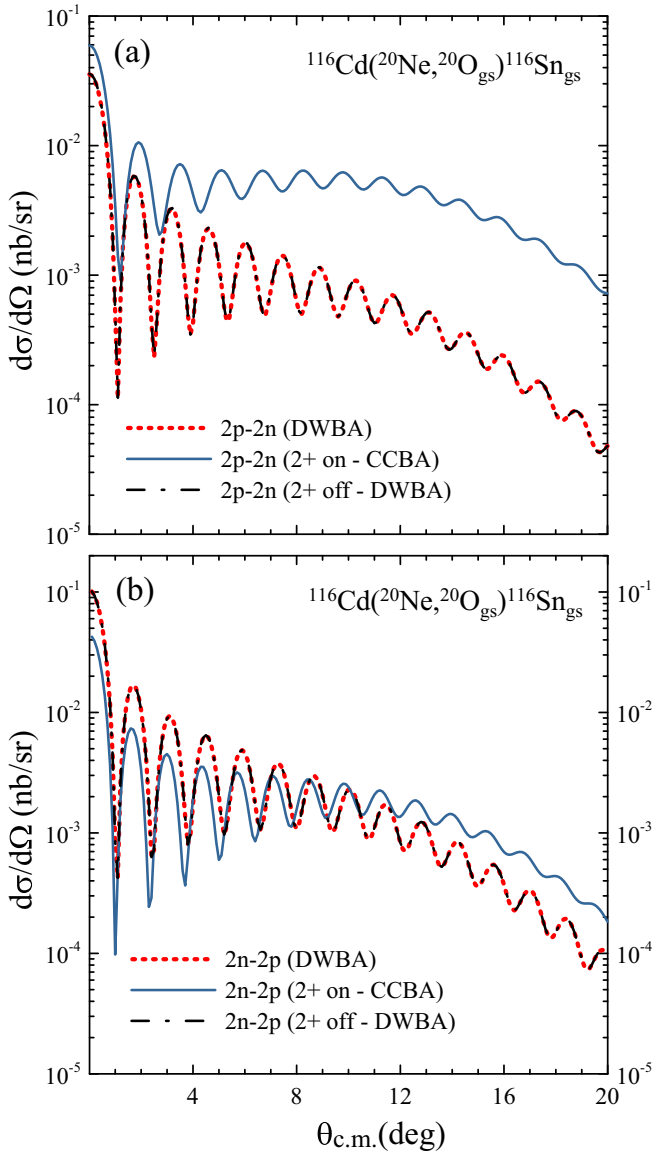

FIG. 5. Theoretical angular distribution for the $^{20}O_{g.s.} + {}^{116}Sn_{g.s.}$ channel corresponding to the paths where the direct two-proton stripping transfer takes place followed by the direct two-neutron pickup reaction and the opposite case, as illustrated in Fig. 1.

The present results, listed in Tables II and III, indicate a very small contribution for the DCE, from the multinucleon transfer mechanism. This agrees with what was stated in Ref. [2] for the case of ^{18}O(^{40}Ca, ^{40}Ar) ^{18}Ne at 15 MeV/u, despite there the conclusion was based on a rather qualitative argument. Thus, one expects a similar behavior for the contribution to DCE from the multi-nucleon transfer mechanism occurring in other systems, such as $^{18}O + {}^{76}Se$, $^{18}O + {}^{116}Sn$, and $^{20}Ne + {}^{130}Te$ in the same energy regime.

Finally, to investigate the relevance of the highest bound excited states of ^{118}Sn in the transition $^{20}Ne + {}^{116}Cd \rightarrow {}^{18}O + {}^{118}Sn \rightarrow {}^{20}O_{g.s.}(0^+) + {}^{116}Sn_{g.s.}(0^+)$, we include some arbitrary excited states with spin $I = 6$–8, and close to the threshold of the two-proton separation energy in ^{118}Sn, which is $S_{2p} = 17.518$ MeV. The spectroscopic amplitudes for the two-particle wave function of these bound excited states were set to 1.0. This approach for the spectroscopic amplitudes of the two-particle wave functions of these arbitrary states, although overestimated, might indicate an upper limit for the strength of the couplings with the highest states of the ^{118}Sn nucleus contributing to the DCE cross section. The obtained theoretical cross section for the $^{20}O_{g.s.}(0^+) + {}^{116}Sn_{g.s.}(0^+)$ channel through this approach is $\sigma_{(2p-2n)} = 1.4 \times 10^{-2}$ nb. This is a still small value for the cross section associated with the DCE from the transfer mechanism, for which the experimental data are of the order of a few nb (see Ref. [2] for ^{40}Ca(^{18}O, ^{18}Ne) ^{40}Ar at 15 MeV/u and [10] for ^{130}Te(^{20}Ne, ^{20}O) ^{130}Xe at 15 MeV/u).

III. CONCLUSIONS

The present study gives for the first time a detailed analysis based on a fully quantum microscopic reaction theory for all the transfer mechanisms that may take place in the double charge exchange reactions. To the best of our knowledge, a similar study has never been carried out even for other systems and at other energy regimes. We present theoretical results for the multinucleon transfer cross sections in the ^{116}Cd(^{20}Ne, ^{20}O)^{116}Sn reaction, at 306 MeV incident energy. This reaction was selected within the NUMEN project aiming at exploring the response to double isospin operators of ^{116}Cd, an isotope candidate to the $0\nu\beta\beta$ decay.

From the multinucleon transfer side, the transition $^{20}\text{Ne} + {}^{116}\text{Cd} \rightarrow {}^{20}\text{O} + {}^{116}\text{Sn}$ can occur by exchanging neutrons and protons between the projectile and target nuclei during the collision. In this case, the dynamics of transfer reaction is governed by the mean-field interaction. The DWBA and CCBA approximations were adopted to analyze the cross sections for the transfer mechanisms. Our calculations are parameter-free since the ISI, FSI, and nuclear structure inputs are not adjusted to our data. Instead, they are constrained by a large body of applications in literature. Even further our technique is constrained by the two-proton and two-neutron transfer analyses performed on the same system adopting the same technique [44] and by elastic/inelastic scattering, one-proton transfer, and single charge exchange in Ref. [19].

We have explored the influence of the couplings of the inelastic states in the initial partition on the transfer cross section. The inclusion of these coupling does not change the conclusion that the theoretical transfer cross sections are very small compared to the experimental data, being at least three orders of magnitude lower. Nevertheless, the transfer from these excited states is more relevant when including higher excited states in the intermediate partitions. The DCE cross section is expected in the range of a few nb, while the largest theoretical multinucleon cross section for this channel is $\approx 10^{-3}$ nb. We thus feel that the DCE experimental cross sections should be analyzed in terms of meson exchange mechanisms, requiring degrees of freedom not considered here. The results of such analyses will be published elsewhere.

The predicted multinucleon transfer angular distributions present a similar oscillating pattern, independently of the routes considered to reach the final partition. This, in turn, indicates that the angular distribution shapes are mainly sensitive to the overall momentum transfer, which does not depend on the specific reaction route. Only the magnitude of the cross section contribution depends on the specific details of each reaction route. We found that the multinucleon transfer starting from the transfer of neutrons, followed by transfer of protons, seems to be more likely than those processes started by transfer of protons. This might be associated with the proton transfer populating high-lying states in the intermediate partition, thus getting unfavorable conditions to populate the low-lying states of the final partition.

Our study shows that the multinucleon transfer mechanism, which occurs at least by a two-step reaction, gives a negligible contribution to the measured DCE cross section. Also, it is worth mentioning that the two-proton and two-neutron transfer cross sections for the ^{116}Cd(^{20}Ne, ^{18}O)^{118}Sn and ^{116}Cd(^{20}Ne, ^{22}Ne)^{114}Cd reactions at 306 MeV, respectively, were well described in Ref. [44]. The agreement between theoretical cross sections and experimental data for these two-proton and two-neutron transfer reactions indicates the feasibility of our method since they are part of the set of transfer reactions feeding DCE.

Although we only have performed transfer calculations for the ^{116}Cd(^{20}Ne, ^{20}O)^{116}Sn reaction, the obtained result is likely not to change qualitatively for other systems, such as those proposed in the NUMEN and NURE projects [1,7]. One should not expect tremendous changes for processes all governed by mean-field and adding so many allowed routes that possible selection rules are largely washed out. These confirmations were stated in Ref. [2] for the ^{18}O(^{40}Ca, ^{40}Ar)^{18}Ne reaction at 15 MeV/u, despite the conclusion being based on a rather qualitative argument.

This result is a milestone for the NUMEN project, demonstrating that the meson exchange is actually the main process feeding the measured DCE. One, of course, cannot distinguish between the exchange of two independent or correlated mesons, which is then a further study to be performed.

ACKNOWLEDGMENTS

This project has received funding from the European Research Council (ERC) under the European Union's Horizon 2020 Research and Innovation Programm (Grant Agreement No. 714625). The authors acknowledge partial financial support from CNPq, FAPERJ, and INCT-FNA (Instituto Nacional de Ciência e Tecnologia - Física Nuclear e Aplicações), Proc. 464898/2014-5.

[1] F. Cappuzzello, C. Agodi, M. Cavallaro, D. Carbone, S. Tudisco, D. Lo Presti, J. R. B. Oliveira, P. Finocchiaro, M. Colonna, D. Rifuggiato *et al.* Eur. Phys. J. A **54**, 72 (2018).

[2] F. Cappuzzello, M. Cavallaro, C. Agodi, M. Bondì, D. Carbone, A. Cunsolo, and A. Foti, Eur. Phys. J. A **51**, 145 (2015).

[3] E. Santopinto, H. García-Tecocoatzi, R. I. Magaña Vsevolodovna, and J. Ferretti, Phys. Rev. C **98**, 061601(R) (2018).

[4] H. Matsubara *et al.*, Few-Body Syst. **54**, 1433 (2013).

[5] K. Kisamori *et al.*, Phys. Rev. Lett. **116**, 052501 (2016).

[6] K. Takahisa, H. Ejiri, H. Akimune, H. Fujita, R. Matumiya, T. Ohta, T. Shima, M. Tanaka, and M. Yosoi, arXiv:1703.08264.

[7] M. Cavallaro *et al.*, PoS BORMIO2017, 015 (2017).

[8] H. Lenske, F. Cappuzzello, M. Cavallaro, and M. Colonna, Prog. Part. Nucl. Phys. **109**, 103716 (2019).

[9] J. I. Bellone *et al.*, Phys. Lett. B **807**, 135528 (2020).

[10] V. Soukeras, F. Cappuzzello, D. Carbone, M. Cavallaro, C. Agodi, L. Acosta, I. Boztosun, A. Brischetto, S. Calabrese *et al.*, Results Phys. **28**, 104691 (2021).

[11] H. Lenske, J. I. Bellone, M. Colonna, and D. Gambacurta, Universe **7**, 98 (2021).

[12] M. Cavallaro, J. I. Bellone, S. Calabrese, C. Agodi, S. Burrello, F. Cappuzzello, D. Carbone, M. Colonna, N. Deshmukh, H. Lenske *et al.*, Front. Astron. Space Sci. **8**, 659815 (2021).

[13] E. N. Cardozo, J. Lubian, R. Linares, F. Cappuzzello, D. Carbone, M. Cavallaro, J. L. Ferreira, A. Gargano, B. Paes, and G. Santagati, Phys. Rev. C **97**, 064611 (2018).

[14] U. Umbelino, K. C. C. Pires, R. Lichtenthäler, V. Scarduelli, G. A. Scotton, A. Lépine-Szily, V. Guimarães, J. Lubian, B. Paes, J. L. Ferreira, M. A. G. Alvarez, J. M. B. Shorto, S. Appannababu, M. Assunção, R. P. Condori, and V. Morcelle, Phys. Rev. C **99**, 064617 (2019).

[15] E. N. Cardozo, M. J. Ermamatov, J. L. Ferreira, B. Paes, M. Sinha, and J. Lubian, Eur. Phys. J. A **54**, 150 (2018).

[16] A. Spatafora, F. Cappuzzello, D. Carbone, M. Cavallaro, J. A. Lay, L. Acosta, C. Agodi, D. Bonanno, D. Bongiovanni, I. Boztosun, G. A. Brischetto, S. Burrello, S. Calabrese, D. Calvo, E. R. ChavezLomeli, I. Ciraldo, M. Colonna, F. Delaunay, N. Deshmukh, J. L. Ferreira, P. Finocchiaro, M. Fisichella, A. Foti, G. Gallo, A. Hacisalihoglu, F. Iazzi, G. Lanzalone, H. Lenske, R. Linares, D. LoPresti, J. Lubian, M. Moralles, A. Muoio, J. R. B. Oliveira, A. Pakou, L. Pandola, H. Petrascu, F. Pinna, S. Reito, G. Russo, G. Santagati, O. Sgouros, S. O. Solakci, V. Soukeras, G. Souliotis, D. Torresi, S. Tudisco, A. Yildirim, and V. A. B. Zagatto, Phys. Rev. C **100**, 034620 (2019).

[17] D. Carbone *et al.*, Universe **07**, 58 (2021).

[18] L. La Fauci *et al.*, Phys. Rev. C **104**, 054610 (2021).

[19] S. Burrello *et al.* (unpublished).

[20] G. Potel, A. Idini, F. Barranco, E. Vigezzi, and R. A. Broglia, Rep. Prog. Phys. **76**, 106301 (2013).

[21] G. Potel, F. Barranco, F. Marini, A. Idini, E. Vigezzi, and R. A. Broglia, Phys. Rev. Lett. **107**, 092501 (2011).

[22] W. von Oertzen and A. Vitturi, Rep. Prog. Phys. **64**, 1247 (2001).

[23] L. Corradi, G. Pollarolo, and S. Szilner, J. Phys. G: Nucl. Part. Phys. **36**, 113101 (2009).

[24] E. Khan, N. Sandulescu, N. V. Giai, and M. Grasso, Phys. Rev. C **69**, 014314 (2004).

[25] Yu. Ts. Oganessian, V. I. Zagrebaev, and J. S. Vaagen, Phys. Rev. C **60**, 044605 (1999).

[26] R. H. Siemssen, C. L. Fink, L. R. Greenwood, and H. J. Korner, Phys. Rev. Lett. **28**, 626 (1972).

[27] H. P. Rother, W. Henning, H. J. Korner, R. Moller, K. E. Rehm, M. Richter, and H. Spieler, Nucl. Phys. A **269**, 511 (1976).

[28] O. Sgouros, M. Cavallaro, F. Cappuzzello, D. Carbone, C. Agodi, A. Gargano, G. DeGregorio, C. Altana, G. A. Brischetto, S. Burrello, S. Calabrese, D. Calvo, V. Capirossi, E. R. ChavezLomeli, I. Ciraldo, M. Cutuli, F. Delaunay, H. Djapo, C. Eke, P. Finocchiaro, M. Fisichella, A. Foti, A. Hacisalihoglu, F. Iazzi, L. LaFauci, R. Linares, J. Lubian, N. H. Medina, M. Moralles, J. R. B. Oliveira, A. Pakou, L. Pandola, F. Pinna, G. Russo, M. A. Guazzelli, V. Soukeras, G. Souliotis, A. Spatafora, D. Torresi, A. Yildirim, and V. A. B. Zagatto, Phys. Rev. C **104**, 034617 (2021).

[29] S. Calabrese, M. Cavallaro, D. Carbone, F. Cappuzzello, C. Agodi, S. Burrello, G. DeGregorio, J. L. Ferreira, A. Gargano, O. Sgouros, L. Acosta, P. Amador-Valenzuela, J. I. Bellone, T. Borello-Lewin, G. A. Brischetto, D. Calvo, V. Capirossi, E. R. ChavezLomeli, I. Ciraldo, M. Colonna, F. Delaunay, H. Djapo, C. Eke, P. Finocchiaro, S. Firat, M. Fisichella, A. Foti, M. A. Guazzelli, A. Hacisalihoglu, F. Iazzi, L. LaFauci, J. A. Lay, R. Linares, J. Lubian, N. H. Medina, M. Moralles, J. R. B. Oliveira, A. Pakou, L. Pandola, H. Petrascu, F. Pinna, G. Russo, S. O. Solakci, V. Soukeras, G. Souliotis, A. Spatafora, D. Torresi, S. Tudisco, A. Yildirim, and V. A. B. Zagatto, Phys. Rev. C **104**, 064609 (2021).

[30] M. C. Lemaire and K. S. Low, Phys. Rev. C **16**, 183 (1977).

[31] M. Bernas, M. Roy-Stephan, F. Pougheon, M. Langevin, G. Rotbard, P. Roussel, J. P. LeFèvre, M. C. Lemaire, K. S. Low, and B. H. Wildenthal, Phys. Rev. C **19**, 2246 (1979).

[32] M. Cavallaro, F. Cappuzzello, M. Bondi, D. Carbone, V. N. Garcia, A. Gargano, S. M. Lenzi, J. Lubian, C. Agodi, F. Azaiez, M. DeNapoli, A. Foti, S. Franchoo, R. Linares, D. Nicolosi, M. Niikura, J. A. Scarpaci, and S. Tropea, Phys. Rev. C **88**, 054601 (2013).

[33] D. Carbone, M. Bondì, A. Bonaccorso, C. Agodi, F. Cappuzzello, M. Cavallaro, R. J. Charity, A. Cunsolo, M. De Napoli, and A. Foti, Phys. Rev. C **90**, 064621 (2014).

[34] A. Parmar, Sonika, B. J. Roy, V. Jha, U. K. Pal, S. T., S. K. Pandit, V. V. Parkar, K. Ramachandran, K. Mahata, S. Santra, and A. K. Mohanty, Nucl. Phys. A **940**, 167 (2015).

[35] F. Cappuzzello *et al.*, Nat. Commun. **6**, 6743 (2015).

[36] M. J. Ermamatov, F. Cappuzzello, J. Lubian, M. Cubero, C. Agodi, D. Carbone, M. Cavallaro, J. L. Ferreira, A. Foti, V. N. Garcia, A. Gargano, J. A. Lay, S. M. Lenzi, R. Linares, G. Santagati, and A. Vitturi, Phys. Rev. C **94**, 024610 (2016).

[37] M. J. Ermamatov, R. Linares, J. Lubian, J. L. Ferreira, F. Cappuzzello, D. Carbone, M. Cavallaro, M. Cubero, P. N. de Faria, A. Foti, G. Santagati, and V. A. B. Zagatto, Phys. Rev. C **96**, 044603 (2017).

[38] D. Carbone, J. L. Ferreira, F. Cappuzzello, J. Lubian, C. Agodi, M. Cavallaro, A. Foti, A. Gargano, S. M. Lenzi, R. Linares, and G. Santagati, Phys. Rev. C **95**, 034603 (2017).

[39] B. Paes, G. Santagati, R. M. Vsevolodovna, F. Cappuzzello, D. Carbone, E. N. Cardozo, M. Cavallaro, H. Garcia-Tecocoatzi, A. Gargano, J. L. Ferreira, S. M. Lenzi, R. Linares, E. Santopinto, A. Vitturi, and J. Lubian, Phys. Rev. C **96**, 044612 (2017).

[40] C. Agodi, G. Giuliani, F. Cappuzzello, A. Bonasera, D. Carbone, M. Cavallaro, A. Foti, R. Linares, and G. Santagati, Phys. Rev. C **97**, 034616 (2018).

[41] R. Linares, M. J. Ermamatov, J. Lubian, F. Cappuzzello, D. Carbone, E. N. Cardozo, M. Cavallaro, J. L. Ferreira, A. Foti, A. Gargano, B. Paes, G. Santagati, and V. A. B. Zagatto, Phys. Rev. C **98**, 054615 (2018).

[42] V. Jha, B. J. Roy, A. Chatterjee, H. S. Patel, B. Srinivasan, M. G. Betigeri, and H. Machner, Eur. Phys. J. A **15**, 389 (2002).

[43] A. Bonaccorso, F. Cappuzzello, D. Carbone, M. Cavallaro, G. Hupin, P. Navrátil, and S. Quaglioni, Phys. Rev. C **100**, 024617 (2019).

[44] D. Carbone, J. L. Ferreira, S. Calabrese, F. Cappuzzello, M. Cavallaro, A. Hacisalihoglu, H. Lenske, J. Lubian, R. I. MagnanaVsevolodovna, E. Santopinto, C. Agodi, L. Acosta, D. Bonanno, T. Borello-Lewin, I. Boztosun, G. A. Brischetto, S. Burrello, D. Calvo, E. R. ChavezLomeli, I. Ciraldo, M. Colonna, F. Delaunay, N. Deshmukh, P. Finocchiaro, M. Fisichella, A. Foti, G. Gallo, F. Iazzi, L. LaFauci, G. Lanzalone,

R. Linares, N. H. Medina, M. Moralles, J. R. B. Oliveira, A. Pakou, L. Pandola, H. Petrascu, F. Pinna, S. Reito, G. Russo, O. Sgouros, S. O. Solakci, V. Soukeras, G. Souliotis, A. Spatafora, D. Torresi, S. Tudisco, A. Yildirin, and V. A. B. Zagatto, Phys. Rev. C **102**, 044606 (2020).

[45] J. L. Ferreira, D. Carbone, M. Cavallaro, N. N. Deshmukh, C. Agodi, G. A. Brischetto, S. Calabrese, F. Cappuzzello, E. N. Cardozo, I. Ciraldo, M. Cutuli, M. Fisichella, A. Foti, L. La Fauci, O. Sgouros, V. Soukeras, A. Spatafora, D. Torresi, and J. Lubian, Phys. Rev. C **103**, 054604 (2021).

[46] H. G. Bohlen, T. Dorsch, Tz. Kokalova, W. von Oertzen, Ch. Schulz, and C. Wheldon, Phys. Rev. C **75**, 054604 (2007).

[47] S. Szilner, L. Corradi, G. Pollarolo, S. Beghini, R. B. Behera, E. Fioretto, A. Gadea, F. Haas, A. Latina, G. Montagnoli, F. Scarlassara, A. M. Stefanini, M. Trotta, A. M. Vinodkumar, and Y. Wu, Phys. Rev. C **71**, 044610 (2005).

[48] E. Vigezzi and A. Winther, Ann. Phys. (NY) **192**, 432 (1989).

[49] A. Winther, Nucl. Phys. A **572**, 191 (1994).

[50] A. Winther, Nucl. Phys. A **594**, 203 (1995).

[51] L. C. Chamon, D. Pereira, M. S. Hussein, M. A. Cândido Ribeiro, and D. Galetti, Phys. Rev. Lett. **79**, 5218 (1997).

[52] L. C. Chamon, B. V. Carlson, L. R. Gasques, D. Pereira, C. De Conti, M. A. G. Alvarez, M. S. Hussein, M. A. Cândido Ribeiro, E. S. Rossi, Jr., and C. P. Silva, Phys. Rev. C **66**, 014610 (2002).

[53] P. P. Tung, K. A. Erb, M. W. Sachs, G. B. Sherwood, R. J. Ascuitto, and D. A. Bromley, Phys. Rev. C **18**, 1663 (1978).

[54] Y. Eisen, H. T. Fortune, W. Henning, F. D. G. Kovar, S. Vigdor, and B. Zeidman, Phys. Rev. C **13**, 699 (1976).

[55] K. E. Rehm, J. Gehring, B. Glagola, W. C. Ma, W. Phillips, and F. L. H. Wolfs, Z. Phys. A **340**, 281 (1991).

[56] P. D. Bond, H. J. Korner, M.-C. Lemaire, D. J. Pisano, and C. E. Thorn, Phys. Rev. C **16**, 177 (1977).

[57] I. J. Thompson, http://www.fresco.org.uk.

[58] I. J. Thompson, Comput. Phys. Rep. **7**, 167 (1988).

[59] L. R. Gasques, L. C. Chamon, P. R. S. Gomes, and J. Lubian, Nucl. Phys. A **764**, 135 (2006).

[60] D. P. Souza, D. Pereira, J. Lubian, L. C. Chamon, J. R. B. Oliveira, E. S. Rossi Jr., C. P. Silva, P. N. de Faria, V. Guimarães, R. Lichtenthaler, and M. A. G. Alvarez, Nucl. Phys. A **836**, 1 (2010).

[61] D. Pereira, J. Lubian, J. R. B. Oliveira, D. P. de Souza, and L. C. Chamon, Phys. Lett. B **670**, 330 (2009).

[62] J. R. B. Oliveira *et al.*, J. Phys. G: Nucl. Part. Phys. **40**, 105101 (2013).

[63] D. Pereira *et al.*, Phys. Lett. B **710**, 426 (2012).

[64] G. R. Satchler and W. G. Love, Phys. Rep. **55**, 183 (1979).

[65] M. El-Azab Farid and G. R. Satchler, Nucl. Phys. A **438**, 525 (1985).

[66] D. T. Khoa, W. von Oertzen, and A. A. Ogloblin, Nucl. Phys. A **602**, 98 (1996).

[67] NUSHELLX for Windows and Linux, http://www.garsington.eclipse.co.uk/.

[68] Y. Utsuno and S. Chiba, Phys. Rev. C **83**, 021301(R) (2011).

[69] R. Machleidt, Phys. Rev. C **63**, 024001 (2001).

[70] R. Machleidt, The meson theory of nuclear forces and nuclear structure, in *Advances in Nuclear Physics*, edited by J. W. Negele and E. Vogt, Advances in Nuclear Physics Vol. 19 (Springer, Boston, MA, 1989), p. 189.

[71] R. Machleidt, K. Holinde, and Ch. Elster, Phys. Rep. **149**, 1 (1987).

[72] D. M. Brink, Phys. Lett. B **40**, 37 (1972).

[73] G. R. Satchler, *Direct Nuclear Reactions* (Oxford University Press, Oxford, 1983).

[74] S. Raman, C. W. Nestor, Jr., and P. Tikkanen, At. Data Nucl. Data Tables **78**, 1 (2001).